

Article

Study on the Influence of Surface Texture Parameters of Oil Production Screw Motor Rotor on the Tribological Properties of Its Friction Pair

Shijin Peng ^{1,*}, Zhiqiang Huang ¹ , Meiling Wang ¹, Chen Xiong ² and Ke Chen ¹¹ School of Mechatronic Engineering, Southwest Petroleum University, Chengdu 610500, China² Shenzhen Mindray Bio-Medical Electronics Co., Ltd., Shenzhen 518055, China

* Correspondence: pengsj8223@gmail.com

Abstract: By researching the influence of micro-groove texture on the surface tribological properties of the stator and rotor pair of oil production hydraulic motors, this paper aims to reduce the frictional resistance moment of the spiral pair of hydraulic motors, and further solve the problem of the difficult restart of the pump of a certain type of hydraulic-driven screw pump. According to the spiral pair of screw motors, a metal-rubber flat plate reciprocating friction model is established, and rectangular micro-grooves with different texture angles and depths are machined on the surface of the metal specimen. A combination of finite element simulation and tribological tests is used to carry out a study on the influence of different texture parameters on the friction performance of the hydraulic motor spiral pair. The results showed that at a certain texture angle, the friction coefficient of each specimen basically increases with the texture depth. When the texture depth is constant, the friction coefficient increases first and then decreases with the increase of the texture angle. The texture angle is the main factor affecting the friction coefficient. Under the same test conditions, the friction coefficient of the textured specimen can be reduced by 20.2% compared with the untextured specimen. In the metal-rubber contact pair of the stator and rotor of the hydraulic motor, the friction reduction mechanism of the texture mainly transport the lubricating medium through the micro-grooves to improve the lubricating conditions. Samples with a reasonable design of texture parameters can effectively reduce the friction coefficient of the friction pair without reducing the service life of the hydraulic motor, which is conducive to the smooth restart of the oil production system of the hydraulically driven screw pump.

Keywords: hydraulic motor; scraping force; finite element simulation; texture parameters

Citation: Peng, S.; Huang, Z.; Wang, M.; Xiong, C.; Chen, K. Study on the Influence of Surface Texture Parameters of Oil Production Screw Motor Rotor on the Tribological Properties of Its Friction Pair.

Processes **2023**, *11*, 618. <https://doi.org/10.3390/pr11020618>

Academic Editor: Qingbang Meng

Received: 1 February 2023

Revised: 13 February 2023

Accepted: 15 February 2023

Published: 17 February 2023



Copyright: © 2023 by the authors. Licensee MDPI, Basel, Switzerland. This article is an open access article distributed under the terms and conditions of the Creative Commons Attribution (CC BY) license (<https://creativecommons.org/licenses/by/4.0/>).

1. Introduction

With the continuous development and maturity of oil and gas exploration and development technology, at present, the oil recovery technologies involved are well-completion technology, stratified water injection technology, artificial lift technology, microbial oil recovery technology, thermal oil recovery technology, nanotechnology, etc. [1–4]. Among them, artificial lifting technology comprises pumping units, screw pumps, electric submersible pumps, gas lifts, and other lifting technology [5–7]. When the oilfield is in the late stage of development, the paraffin and asphaltenes produced can cause many problems to the normal production of oil wells. Many wax-containing substances will accumulate on the pipe wall, reducing the oil flow area and leading to blockage and other problems, which can even lead to production stoppage in serious cases and affect oil recovery efficiency [8,9]. However, due to structural reasons, the dominant pumping unit lifting technology system efficiency is low, with high energy consumption. The screw pump, because of its compact and simple structure, low energy consumption, and high pumping efficiency for high wax, high sand, high gas crude oil and in slanting wells, horizontal wells, swampy blocks, and

offshore platforms with unique superiority make it widely used, and its status is second only to the century-old pumping lift technology [10,11].

The hydraulic motor is one of the important power transmission parts in the screw pump production system. Under the conditions of low speed and heavy load, it is difficult to establish the oil film on the surface of the hydraulic motor moving pair, which in turn leads to the increase of friction between the moving pair of hydraulic motors, reducing the mechanical efficiency of the hydraulic motor and increasing the cost of oilfield exploitation. Therefore, the harsh lubrication conditions on the surface of the moving pair of hydraulic motors are an important factor limiting the cost reduction and efficiency improvement of the oilfield [12]. However, at present, the research on the key technologies of reducing friction and drag on the surface of the hydraulic motor friction pair mostly focuses on the structural design [13–15], the surface coating [16–18], and the chemical modification of the rubber stator surface [19–22]. The friction reduction effect is achieved mainly by changing the material properties of the friction pair, but the lubrication between the friction pair is not improved.

Texturing treatment is a surface modification technology that can improve the tribological properties of matching pairs by processing micro-morphologies with specific shape and size characteristics on the surface of materials through ultra-precision machining [23–26]. The surface micro-texture under boundary lubrication conditions can act as a storage lubricant medium and provide “secondary lubrication” to the contact surface. Currently, it is mainly applied to pistons [27,28], cutting tools [29], sliding bearings [30], computer hard disks [31], and other surfaces. Pettersson et al. used the embossing process for texture in piston-roller friction pairs of reciprocating hydraulic motors and found that the texture angle had a large effect on the tribological properties of the treated specimens [32]. Edachery, Vimal et al. explored the fluidity and adsorption ability of texture angle on the engineering surface lubricant and found that when the texture angle is parallel to the flow direction, the fluidity is better [33]. Zhang, Li et al. studied the effect of areal density on the wear and drag reduction effect of texture, and found that the best tribological properties can be obtained when the areal density is 10% [34,35]. Su, Liu et al. explored the mechanism of the effect of groove texture depth on the tribological properties of stainless steel surfaces under oil lubrication and found that the texture depth had a significant effect upon contact with the tribological properties, and the best tribological properties were obtained for the mating surfaces when the texture depth was 10 μm [36,37]. He et al. studied the influence of texture edge protrusions on the tribological properties of matching pairs and found that the texture with edge protrusions would aggravate its friction and wear [38]. Zhenhai Xu, Ze Wu et al. discovered that controlling the processing quality of surface texture can effectively improve the wear and drag reduction performance of texture specimens [39,40]. Dzyura and Maruschak et al. investigated the variation patterns of workpiece surface quality under different operation techniques, and the results showed that good operation techniques can obtain a suitable roughness surface and thus improve the serviceability characteristics of the parts [41,42]. Although scholars have carried out a large number of experimental studies on the tribological properties of texture treatment in friction behavior, it is generally believed that the friction reduction mechanism is the dynamic pressure lubrication effect generated by the lubricating medium in the micro-grooves [43–45].

In summary, few scholars have researched the surface texture treatment of the metal-rubber pair of hydraulic motors. Compared with metal contact pairs, the friction situation in metal-rubber contact pairs is more complex and needs more in-depth research. The introduction of surface texture technology to improve the surface tribological properties of metal-rubber mating pairs has strong engineering significance.

To this end, the goal and objective of this study is to introduce texture technology to improve and solve the start-up difficulties in screw pump production systems. In this work, a 42CrMo-nitrile butadiene rubber (NBR) flat plate reciprocating model is established according to the actual working conditions of the hydraulic motor, and the finite element simulation and tribological test methods are used. The influence of different

texture parameters on its tribological properties was studied, and the friction reduction mechanism of texture in the metal-rubber pair of screw motors was analyzed. It provides ideas for solving the problem of difficulty in the start-up of the oil production system of the hydraulically driven screw pump after shutdown.

2. Tribological Test and Model Construction

2.1. Structure of Hydraulic Motor

The focus of this study is to explore whether the introduction of surface micro-texture into metal-rubber pairs under interference fit conditions can be a new design direction to solve the problem of the difficulty of restarting the hydraulic motor after shutdown. However, the structure of the hydraulic motor is complex, and it is impossible to complete the test according to the actual model with the existing laboratory equipment conditions. Therefore, in this study, the actual material characteristics and assembly conditions of the hydraulic motor are kept unchanged, and the spiral metal-rubber pairing is simplified to a flat metal-rubber pairing to study the influence of the rotor surface texture parameters on the tribological performance of the oil exploitation hydraulic motor. The simplified route is shown in Figure 1.

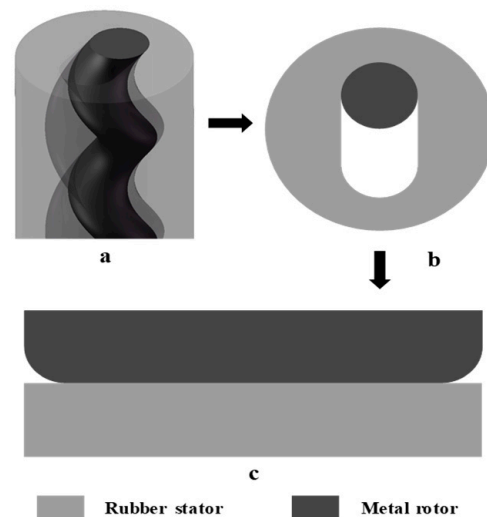


Figure 1. Model simplification. (a) Screw pump 3D model (b) Two-dimensional simplified model (c) Simplified reciprocating model.

This time, the experimental study on the tribological properties of the surface texture treatment of the screw motor rotor was carried out. The purpose is to simulate the tribological properties of a screw pump shut down after a time when the texture is introduced. Therefore, the selected metal rotor material is 42CrMo alloy and the rubber stator material is nitrile rubber. Tables 1 and 2 show the important material parameters of the selected materials.

Table 1. Physical parameters of rotor alloy steel.

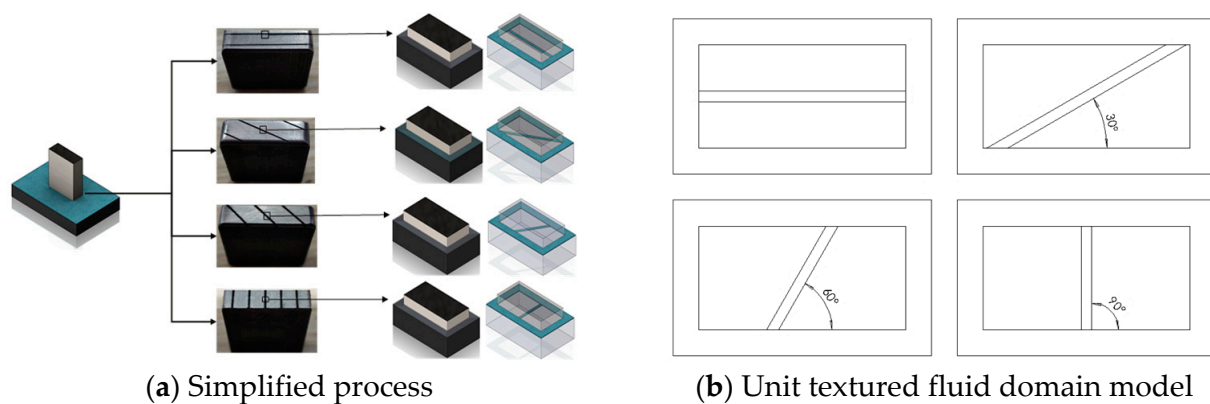
Density kg/m ³	Elasticity Modulus MPa	Poisson Ratio
7800	2.1×10^5	0.3

Table 2. Super elastic physical parameters of stator rubber bushing.

Density kg/m ³	Elasticity Modulus MPa	Poisson Ratio	Material Constant C ₁₀ /MPa	Material Constant C ₀₁ /MPa
1200	11.49	0.4996	1.879	0.038

2.2. Establishment of Simulation Model for Texture

To explore the influence of different texture angles and depths on the conveying capacity of the lubricating medium, a unit-textured fluid domain model was established with the simplified process shown in Figure 2. The size of the test sample is fixed, so the length of the texture on the plane is automatically determined by the determined texture angle.

**Figure 2.** Simplified process and unit textured fluid domain model.

The fluid parameters and editing conditions of the lubricating medium fluid domain in the unit texture are set as follows:

The density of the lubricating medium in the unit texture structure is 827 kg/m³, and the dynamic viscosity is 0.02514 N · s/m². The flow state of the lubricating medium in the unit texture is set to laminar flow. The laminar model was set up in Abaqus as the computational model for the fluid in the cell texture, and the contact form was “hard” contact, with the rotor surface as the primary surface and the stator surface as the slave surface. At the same time, the mesh quality was checked, and the average mesh quality of the textured fluid domain model of this element was 0.84 (the maximum was 1), which met the calculation requirements, and there were 140,776 mesh elements in total. The upper wall is set as a slip interface with a sliding velocity of 100 mm/s, the entrance and exit are set as periodic boundary conditions, and the lower wall is set as no slip. By simulating and analyzing the flow rate of the lubrication medium in the micro-groove model under different texture parameters, the influence of the texture parameters on the transport capacity of the lubrication medium was judged, and the influence law of the micro-grooves under different texture parameters on the motion of the lubrication medium was obtained.

To grasp the influence of the texture topography parameters of the textured rotor on the scraping ability of the rubber stator, the three-dimensional simulation model of 42CrMo alloy and nitrile rubber material shown in Figure 3 was established.

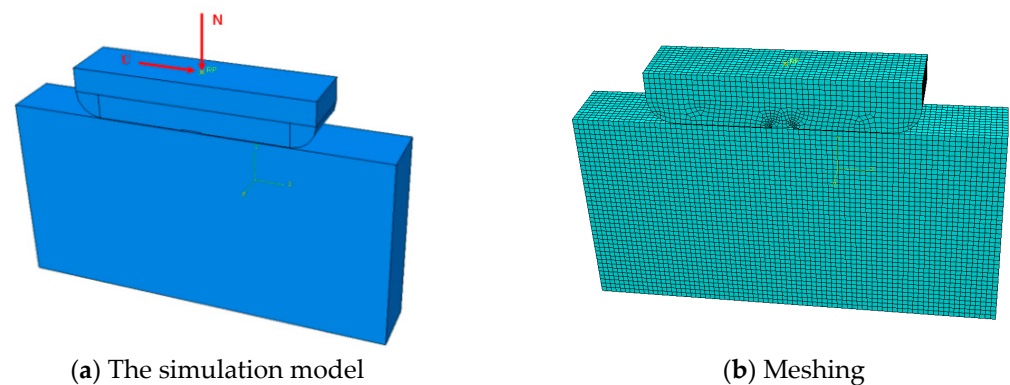


Figure 3. Simplified 3D model of flat plate reciprocation and meshing.

The boundary conditions of the flat plate reciprocating simplified 3D model are set as follows:

The lower specimen material was selected as NBR and the upper specimen material was selected as 42CrMo alloy. The material properties are shown in Tables 1 and 2, and the Mooney–Rivlin constitutive model was chosen to characterize the hyperelasticity of the NBR material. In order to study the effect law of grooves on rubber surface stress under different texturing parameters and ignoring the effect of friction, a 42CrMo–NBR contact pair is established, a fixed constraint is applied to the lower surface of the rubber specimen, and a vertical downward displacement of 0.3 mm is added to the upper surface of the metal specimen to achieve an interference fit. Then, a horizontal displacement of 0.3 mm is applied to the metal specimen after the interference fit is completed.

$$W = C_{10}(I_1 - 3) + C_{01}(I_2 - 3) \quad (1)$$

where C_{10} and C_{20} are the characteristic parameters of the material.

2.3. Tribological Tests

2.3.1. Experimental Design

To grasp the drag reduction effect of the micro-texture under different parameters, the UMT-Tribolab friction and wear testing machine shown in Figure 4 was used to conduct the tribological test and extract the friction force under different texture parameters.

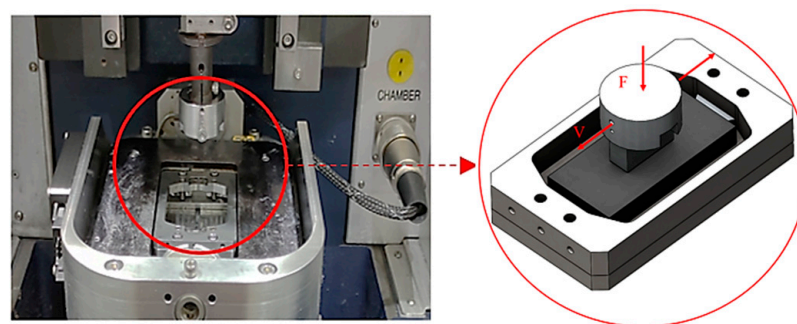


Figure 4. Test equipment.

To simulate the start-up process of the hydraulic motor, the flat plate reciprocating motion module is used to carry out the test; that is, the speed of the upper specimen increased from 0 to the maximum value and then gradually decreased to 0 in a periodic motion, simulating the start-stop state of the test piece twice in one motion cycle. Table 3 shows the table of the levels of factors influencing the orthogonal test and the test equipment selected in this study. The 42CrMo metal block upper test piece simulates the metal

rotor and the 60HA hardness NBR lower test piece simulates the rubber stator. The selected specimen materials were consistent with the hydraulic motor materials with starting difficulties.

Table 3. Influence factor level of orthogonal test.

Level	Factors	
	Angle/°	Depth/ μm
1	0	5
2	30	10
3	60	15
4	90	20

The lubricating medium chosen for this test is the 600XP220 lubricant produced by Mobil Corporation in Jiangsu Province, mainland China, and the test load F is 79.844 N, according to the interference amount of the hydraulic motor. Since the purpose of this research is to improve the starting performance of the hydraulic motor, the state change from static to motion is mainly considered, and the speed requirement is not high, so the default linear reciprocating stroke of 5.0 mm is selected for the test bench, as is the maximum 10 mm/s Linear velocity V , friction time 1200 s, and room temperature.

The data is automatically recorded by the computer during the test. Each group of tests was carried out three times. The average value of the three experimental data was taken as the final friction and wear test result, and the ratio of friction force to load at each time point was taken as the friction coefficient.

2.3.2. Specimen Preparation

Among many surface texturing technologies, laser processing technology is the most widely used because of its advantages of high precision, low cost, low pollution, and high efficiency [46]. Before laser processing, the metal specimen is roughed with a grinder, and then a wire-cutting machine cuts the metal sample into small pieces that meet the size requirements of the testing machine. Then, the surface of the specimen is filleted to simulate the contact between the stator and the rotor. The number of texturing tests required in this study is small. Under the condition of ensuring the processing accuracy, the YLP-20W fiber laser marking machine was selected to process the 42CrMo surface after rough grinding, as shown in Table 4 (the left number in the code indicates the texturing angle and the right number indicates the texturing depth), keeping the width $W = 400 \mu\text{m}$ and the area ratio 10% constant, with the groove-shaped texturing angle and depth as variables [23,34,36,45]. The laser processing parameters are as follows: processing speed 300 mm/s, power 15 W, and laser frequency 20 KHz.

Table 4. Sample number.

Angle \ Depth	Depth			
	5	10	15	20
0	0–5	0–10	0–15	0–20
30	30–5	30–10	30–15	30–20
60	60–5	60–10	60–15	60–20
90	90–5	90–10	90–15	90–20

By changing the placement angle of the specimen on the workbench of the laser marking machine to change the texture angle, under the influence of the laser thermal shock effect, the periphery of the texture will cause a bump. At this time, after the groove is machined and formed, the grinder-treated specimen is polished again with 2000-grade sandpaper to reduce the influence of the texture edges and obtain a metal specimen that

meets the surface roughness requirements of the metal rotor of the hydraulic motor, as shown in Figure 5.

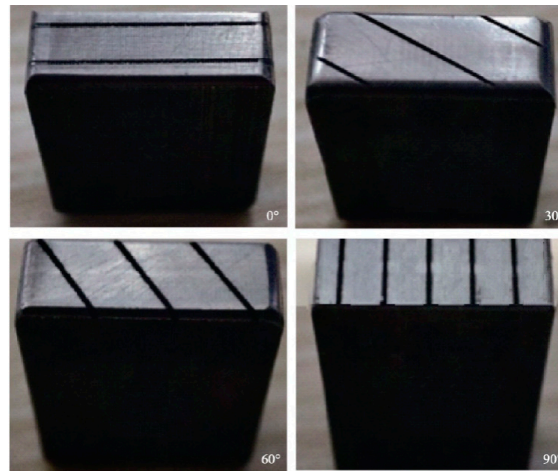


Figure 5. Textured specimens at different angles.

By changing the laser processing times to control the texture depth, the processing times selected in this experiment are 1, 3, 5, and 7, respectively. The texture morphology was observed by the ContourGT InMotion 3D optical microscope to obtain the surface profile shown in Figure 6. From the observation results, the groove depths h corresponding to different processing times were 5, 10, 15, and 20 μm , respectively.

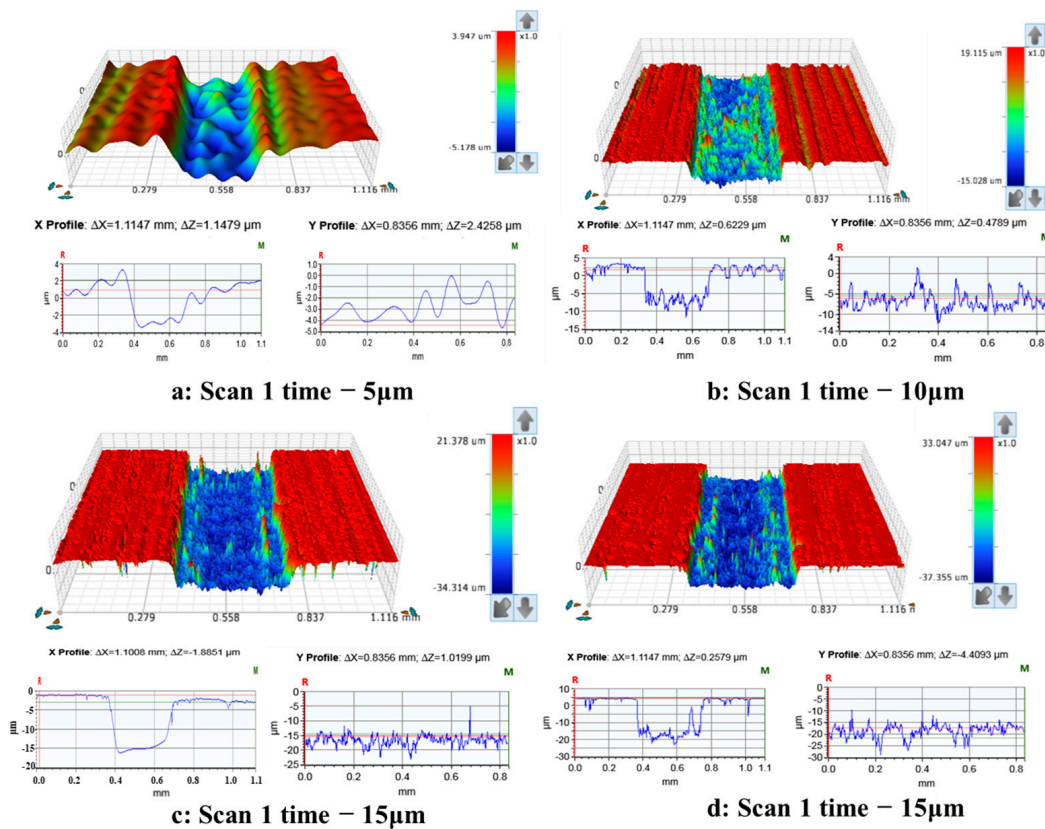


Figure 6. Texture depth corresponding to different scan times.

3. Results

3.1. Effect of Texture Angle on Tribological Properties

3.1.1. The Influence of Texture Angle on the Transport Capacity of the Lubricating Medium

Research on the tribological characteristics of screw pumps has focused on the effects of friction factors, overfill, and operating differential pressure on rubber contact wear [1]. This paper is the first to study the start-up of a screw pump by introducing the texturing technique, and analyzing the laws of friction coefficients, lubricating media, and scraping and cutting forces on rubber contact wear in the presence of texture. The lubricating medium flow line of the screw motor stator during the texturing process for each texturing parameter is shown in Figure 7. Extraction of the lubricating medium flow rate at the cross section in the unit texture was conducted for subsequent analysis.

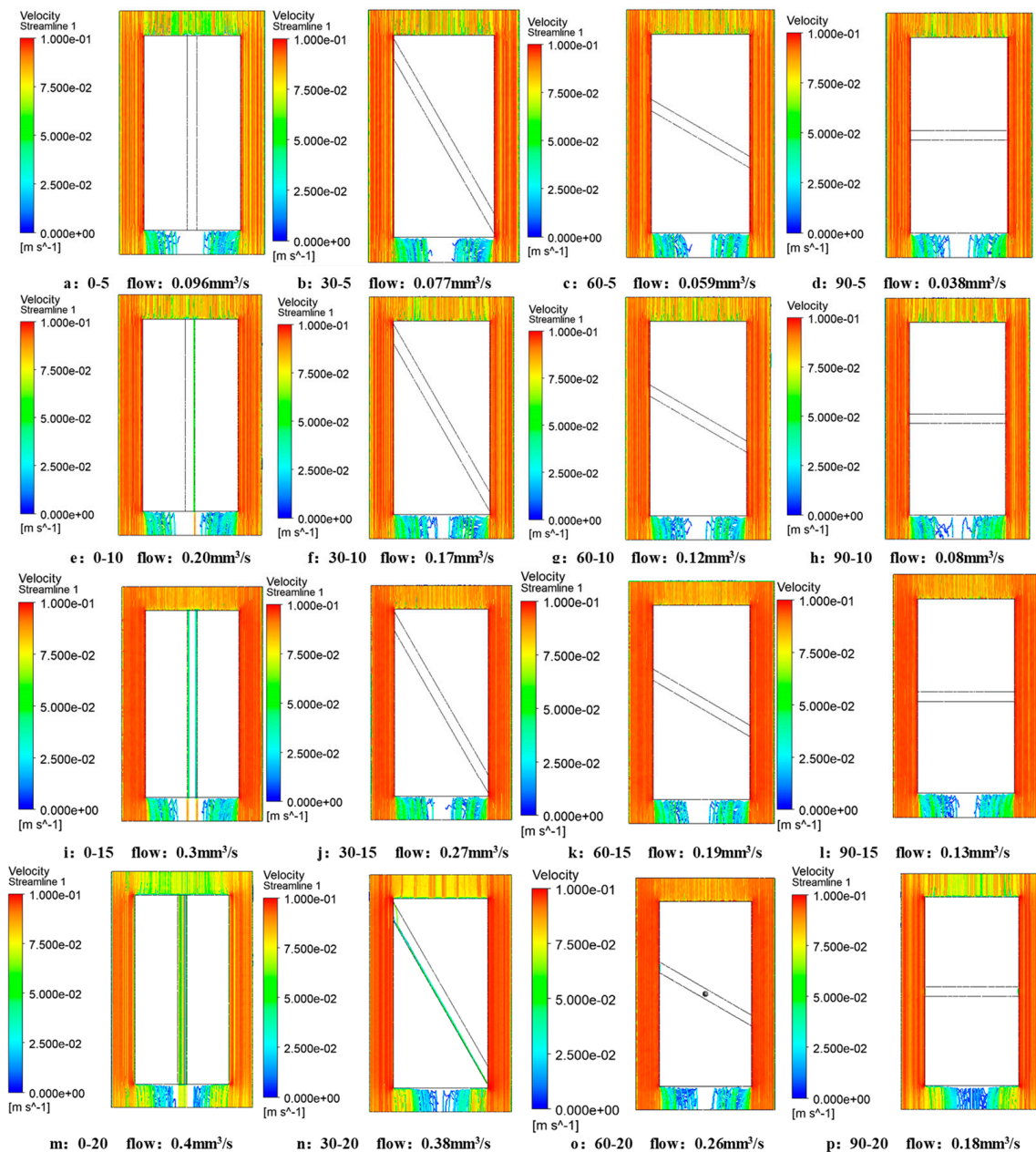


Figure 7. Flow diagram of lubricating medium with different texture parameters.

Figure 8 shows the effect of the change of texture angle on the flow rate of the lubricant medium in the texture of each group of specimens under the same texture depth. From the general trend, the flow rate of the lubricating medium at the cross-section in each depth texture shows a decrease with increasing angle. When the texture angle is 0° , the maximum flow rate of the lubricating medium is obtained, and when the texture angle is 90° , the minimum flow rate of the lubricating medium is obtained. Therefore, when the scraping effect of the texture on the rubber is not considered, the arrangement direction of the texture should be consistent with the relative movement direction between the specimens; that is, the texture angle should be 0° to ensure that the surface of the matching pair has better lubrication conditions.

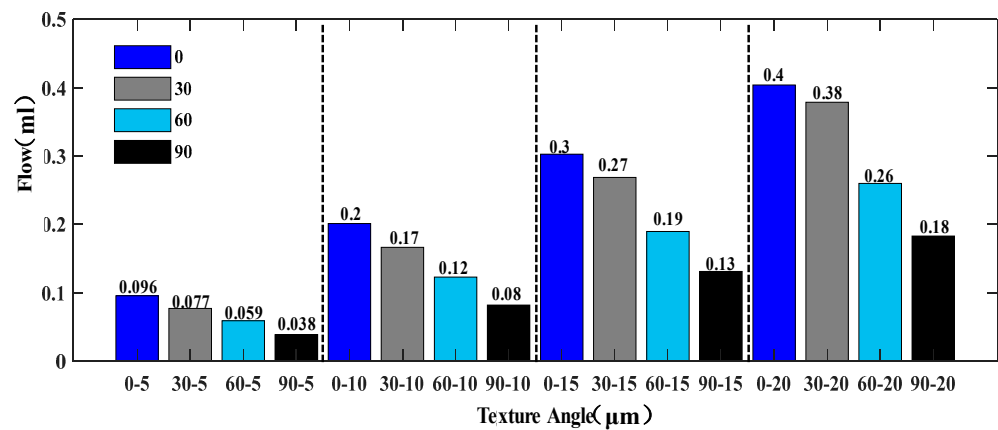


Figure 8. The effect of angle change on the flow rate of the lubricating medium in the textured cross-section of each group of specimens under the same texture depth.

Figure 9 is a schematic diagram of the lubricating medium passing area under different weaving angles based on the simulation results of the effect law of weaving angle on the transport capacity of the lubricating medium. Since the motion direction of the upper metal specimen set in this study is consistent with the longitudinal direction, it is known that the smaller the included angle between the texture angle and the motion direction of the lubricating medium, the easier it is for the lubricating medium to flow through the micro-groove through the metal-rubber mating contact area under the interference fit condition. When the texture density is the same (the texture density selected for the test is 10%), and the smaller the included angle is, the easier it is for the lubricating medium to enter the contact surface, and the larger the contact area that can pass through. When the texture angle is 90° , there is no lubricating medium on the contact surface, the lubrication condition is the worst, and the friction coefficient of the friction pair is the largest. When the texture angle is 0° , the lubricating medium can pass through the whole contact surface, the lubrication condition is the best, and the friction coefficient of the friction pair is the minimum.

3.1.2. The Effect of Texture Angle on Scraping Force

Figure 10 is the maximum scraping force extracted from Figure 11, and each set of data describes the effect of texture angle changes on the scraping force when the texture depth is $5 \mu\text{m}$, $10 \mu\text{m}$, $15 \mu\text{m}$, and $20 \mu\text{m}$, respectively. Observing and comparing the data of each group, we can see that the texture angle-scraping force curves at different texture depths all show a trend of increasing first and then decreasing. The maximum scraping force is obtained when the texture angle is 60° , which has the most hindered relative motion of the mating pairs. As can be seen from figure which shows the laws of the effect of variation of texture depth on the friction coefficient of each test group under the same conditions of texture angle, with the increase of the texture angle, the reduction amount of the rubber scraping force inside the texture relative to the rubber scraping

force at the texture boundary gradually increases. This indicates that as the texture angle increases, more rubber is embedded in the texture, more rubber is damaged by the scraping action, and the more significant the service life reduction effect is of the rubber stator of the progressing screw pump.

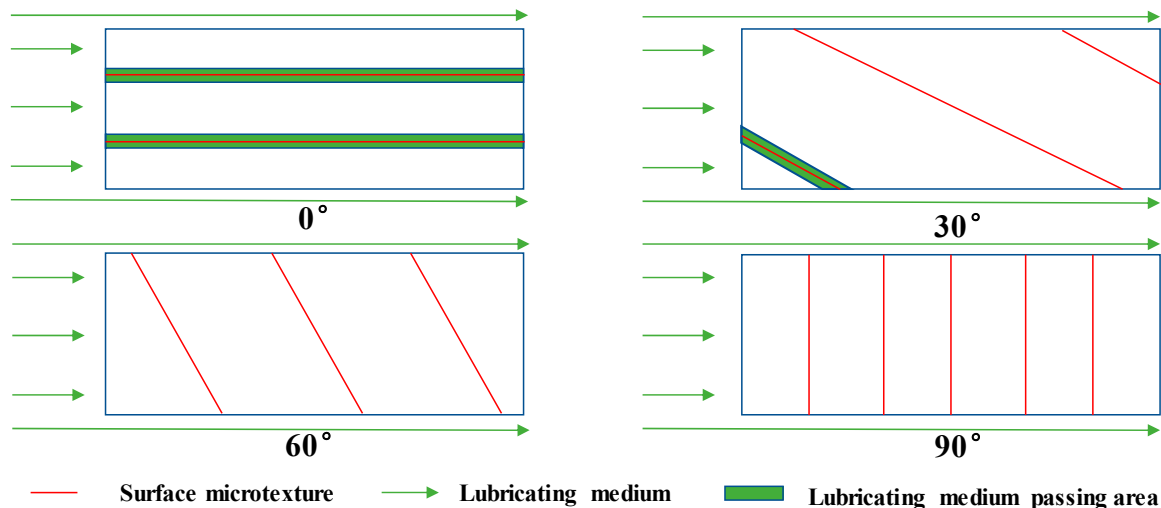


Figure 9. Lubricating medium passing area under different texture angles.

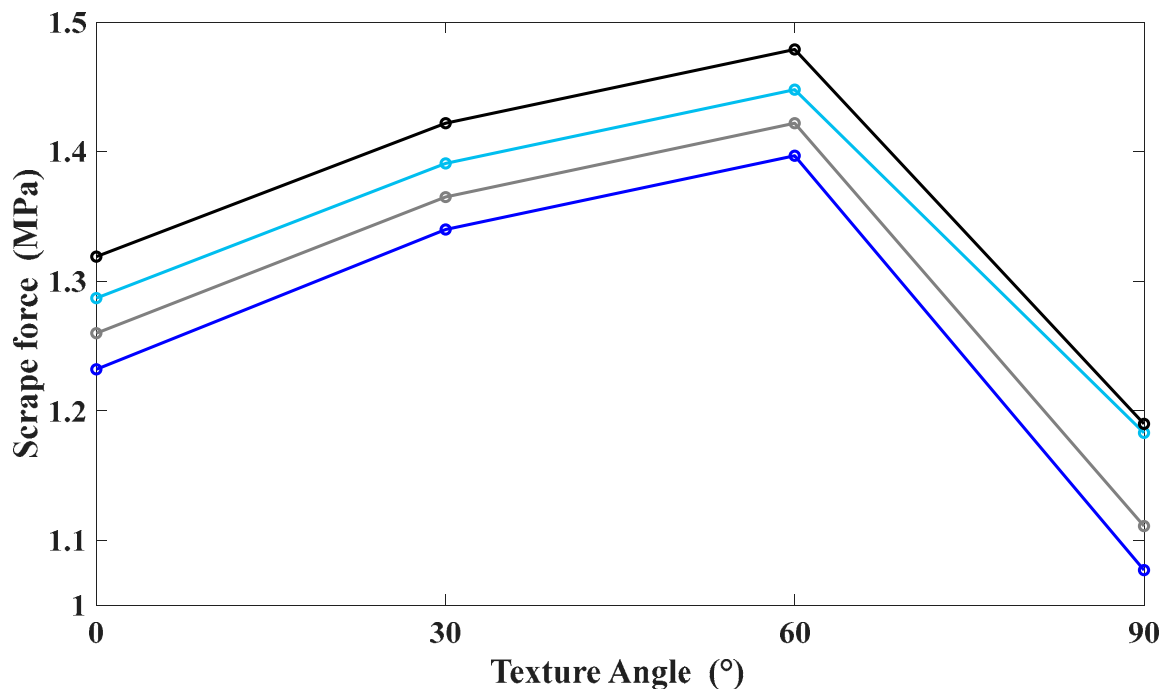


Figure 10. The effect of depth change on the scraping force of each group of specimens when the texture angle is constant.

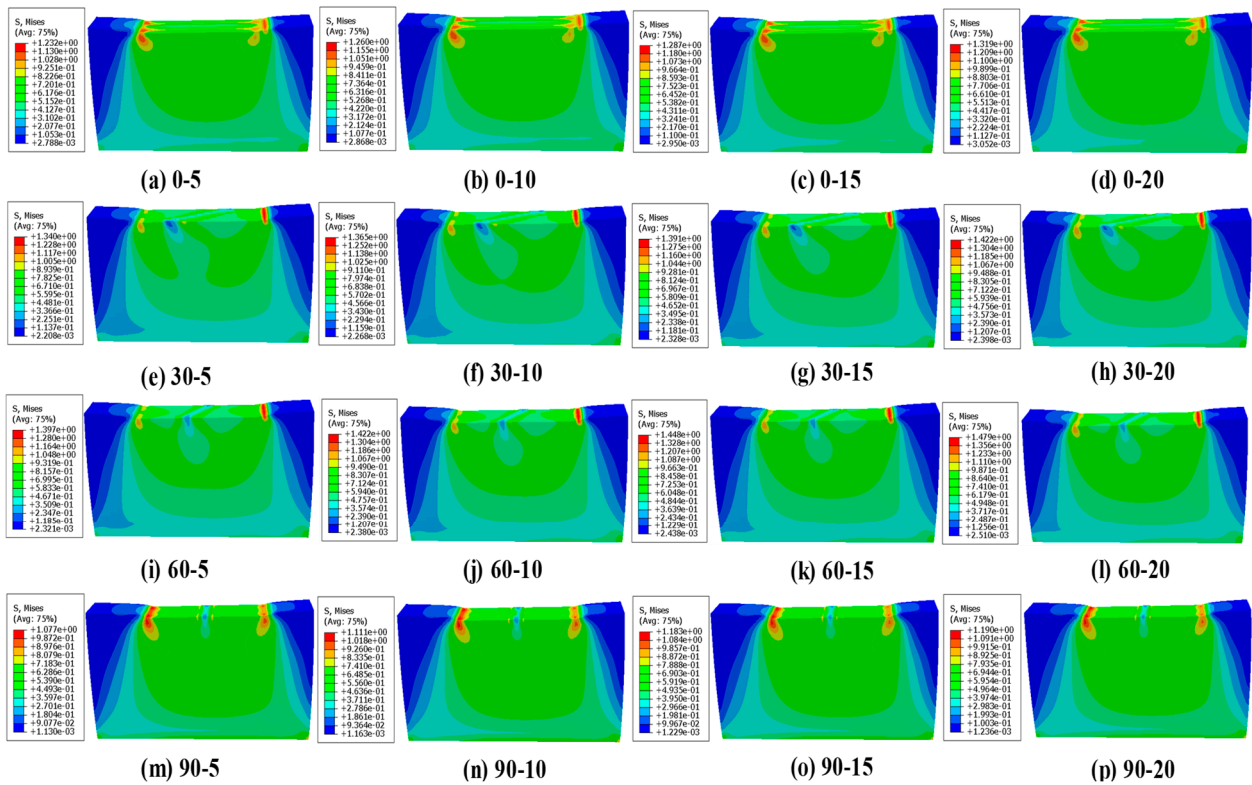


Figure 11. Stress distribution on the rubber surface.

3.1.3. Effect of Texture Angle on Friction Coefficient

From Figure 12a–d, it can be seen that the friction coefficients of each sample tend to reach a steady state after 600s. The arithmetic means that the value of solving for the stabilized friction coefficient of each group of specimens goes in Figure 12e. The experimental results show that, except for the sample with the texture depth of 5 μm , the friction coefficient of each sample increases first and then decreases with the increase of the texture angle, and reaches the maximum value when the texture angle is 60° and reaches the minimum value when the texture angle is 0° . However, the maximum friction coefficient mostly occurs in the experimental group when the texture angle is 60° instead of the experimental group at 90° . This is because the change in the angle of the texture will trigger changes in both the ability to scrape the rubber and the ability to transport the lubricating medium. When the texture angle is 60° , the scraping rubber ability of the matching pair reaches the maximum, and the obstruction ability of the matching pair movement is the strongest.

3.2. Effect of Texture Depth on Tribological Properties

3.2.1. Effect of Texture Depth on Lubricating Medium Transport Capacity

Figure 13 shows the influence of the change of texture depth on the flow rate of the lubricating medium in the textured section of each group of specimens under the same texture angle. By comparing and analyzing the flow rate of the lubricating medium at the cross-section of the texture at each angle, it can be found that the flow rate of the lubricating medium at the cross-section of the texture at each angle increases with the increase of the depth. There is almost no change in the flow rate difference when the texture depth changes from 5 μm to 20 μm at each angle. The difference is that the smaller the texture angle is, the greater the influence of texture depth on the flow of lubricating media is in the cross-section.

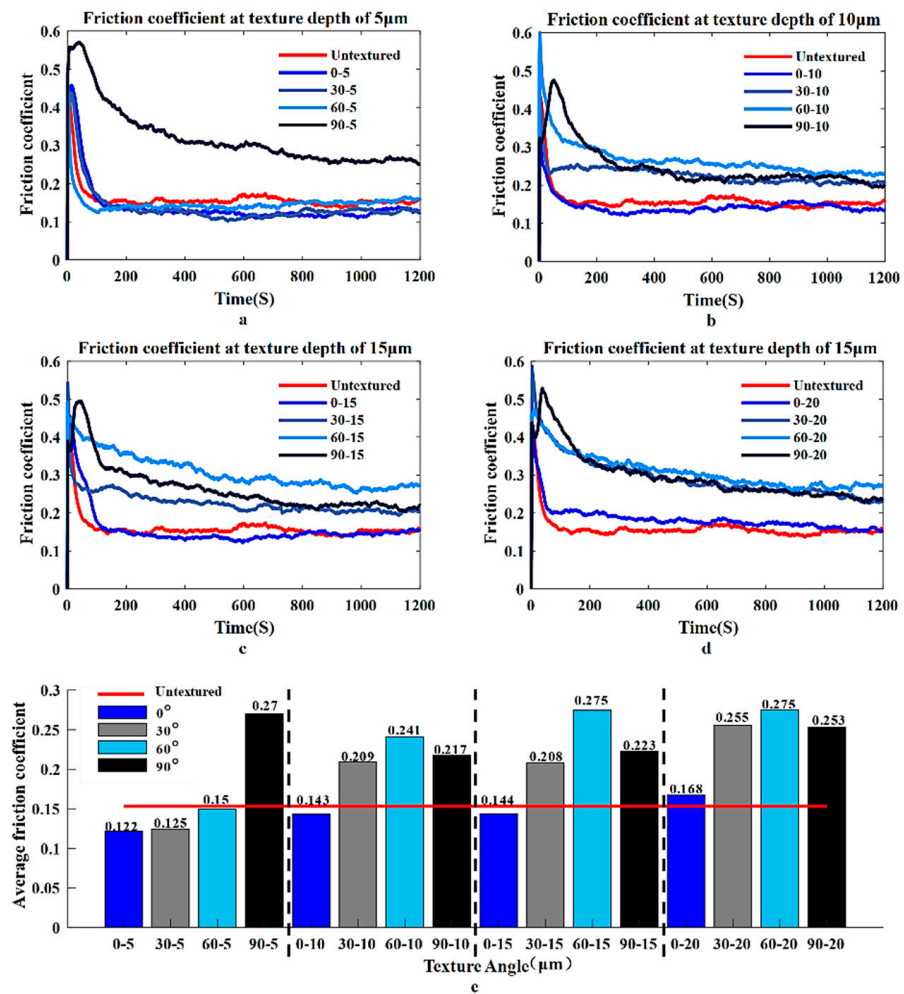


Figure 12. Influence of texture angle change on friction coefficient of each experimental group under the same conditions of texture depth. (a) Friction coefficient at texture depth of 5 μm (b) Friction coefficient at texture depth of 10 μm (c) Friction coefficient at texture depth of 15 μm (d) Friction coefficient at texture depth of 20 μm (e) Average friction coefficient at different texture angles.

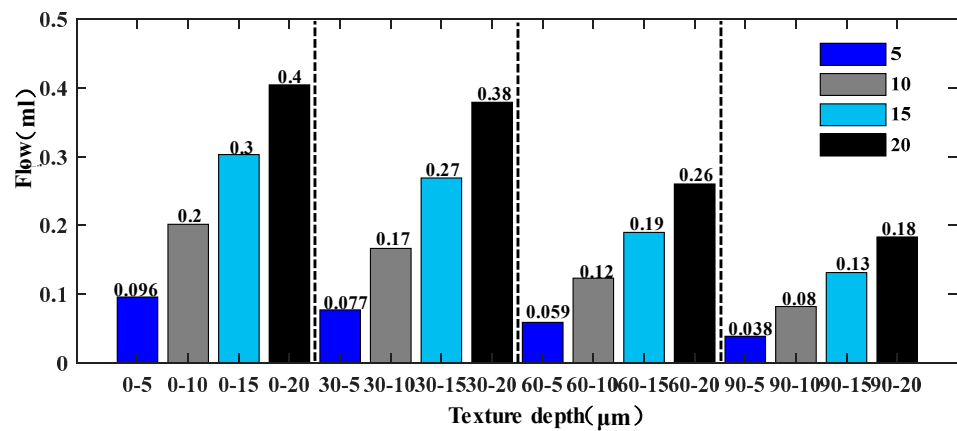


Figure 13. The effect of depth variation on the flow rate of the lubricating medium in the cross-section of each group of specimens under the same conditions of texture angle.

3.2.2. Effect of Texture Depth on Scraping Force

Figure 14 shows the scraping stress on the rubber surface extracted from each group of specimens, and it can be observed that the rubber on the value path is affected by the

abrupt change in the shape of the micro-groove boundary, and the stress concentration phenomenon appears. When the texture angle is 0° to 60° , the scraping force of each group of specimens increases with the increase of texture depth, and the increase was stable among the depths. When the texture angle is 90° , the scraping force increases significantly between the texture depth of $10\ \mu\text{m}$ and $15\ \mu\text{m}$, and the scraping force is approximately equal when the texture depth is $15\ \mu\text{m}$ and $20\ \mu\text{m}$.

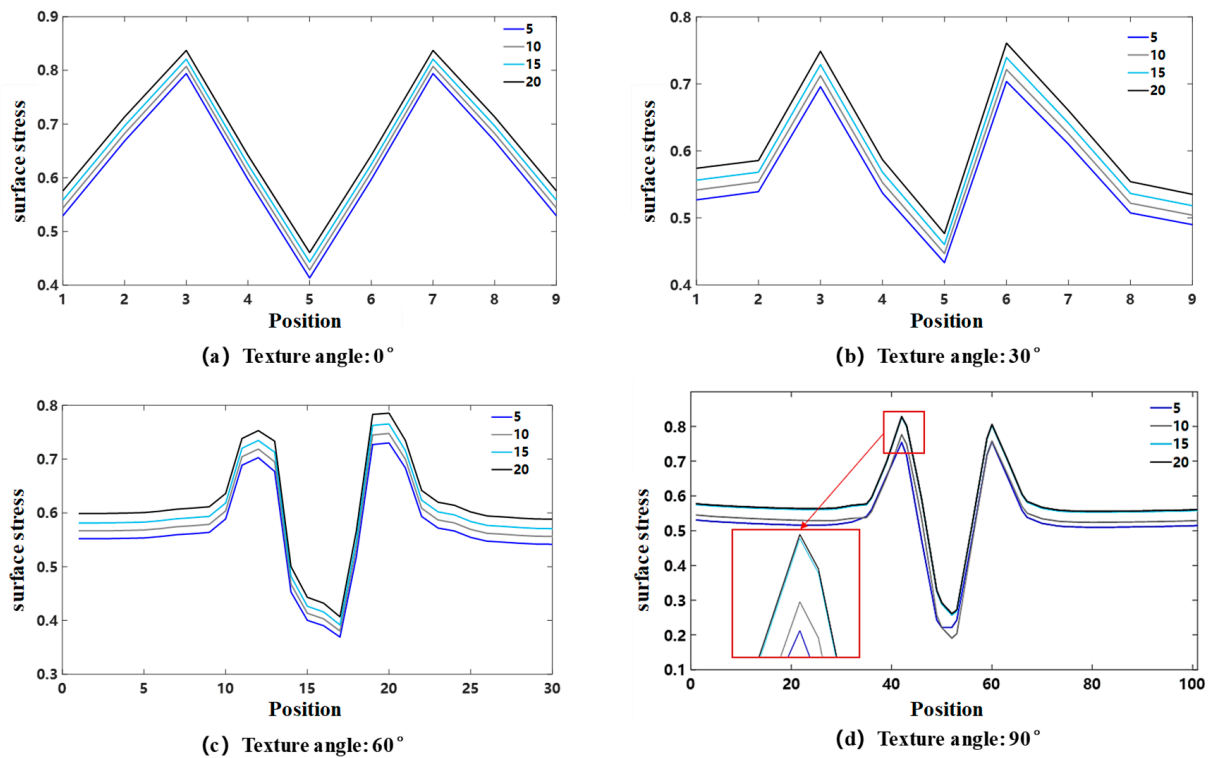


Figure 14. Scraping stress on rubber surface under the same conditions of texturing angle.

3.2.3. Effect of Texture Depth on Friction Coefficient

Figure 15a–d show the laws of the effect of variation of texture depth on the friction coefficient of each test group under the same conditions of texture angle. The friction coefficients of the other groups of specimens all show the characteristic that the maximum static friction force gradually decreases and finally tends to be stable. This is because when the weaving angle is 90° , the micro-groove displays a negligible oil delivery capacity, the lubrication state on the contact surface is dry friction, and the rubber is directly embedded inside the micro-groove by elastic deformation at the beginning of the movement. Since the rubber wears a lot, and the rubber embedded inside the micro-groove is completely scraped off at about 50 s, the friction coefficient of each specimen begins to decrease gradually.

Figure 15e shows the histogram of the average friction coefficient of each group of specimens after stabilization. The test results show that, except for the No. 90-5 specimens, when the texture angle is constant and the texture depth changes, the friction coefficient of each group of specimens shows a phenomenon that increases with the increase of the texture depth. This is because as the texture depth increases, the amount of rubber embedded in the micro-grooves also increases, and the ability to hinder the movement of the contact pair is stronger.

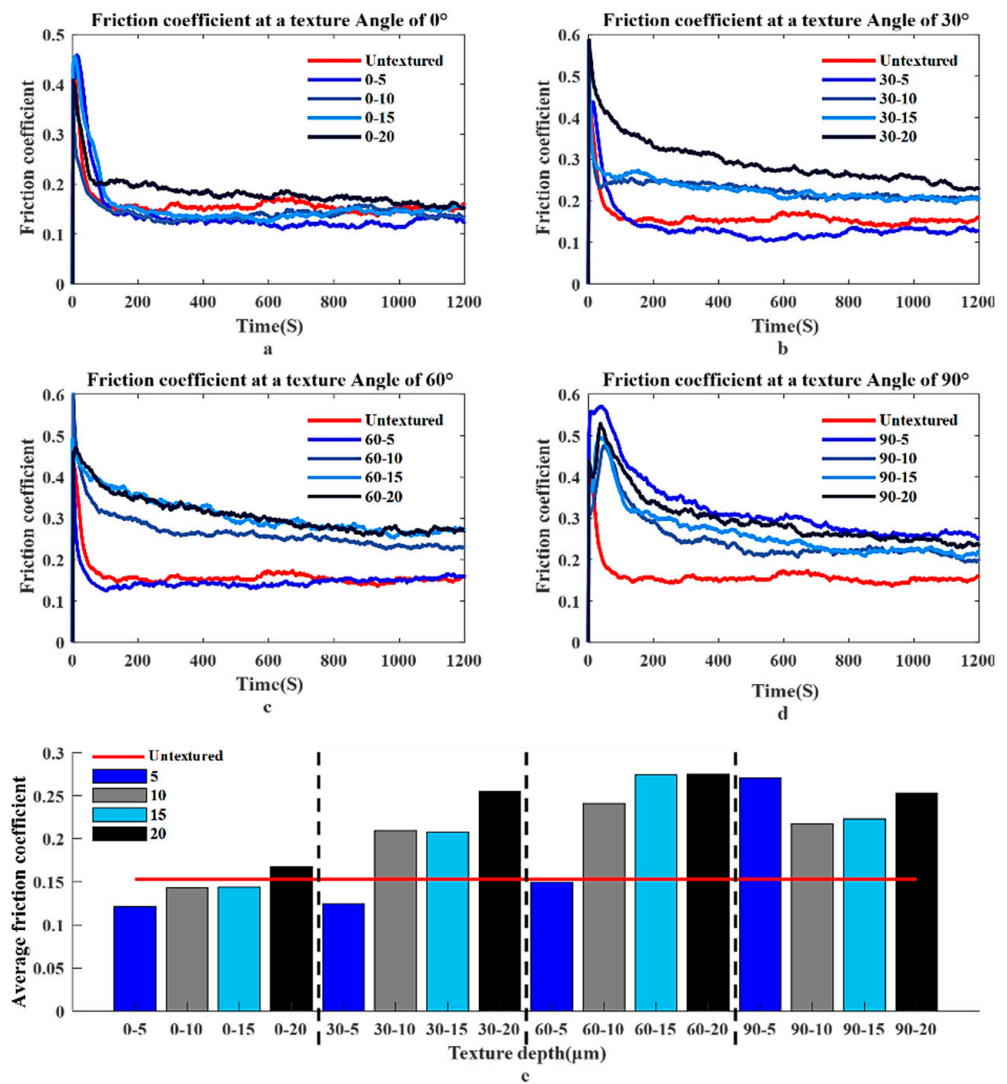


Figure 15. The effect of depth change on the friction coefficient of each test group under the same conditions of texturing angle. (a) Friction coefficient at texture angle of 0° (b) Friction coefficient at texture angle of 0 (c) Friction coefficient at texture angle of 0° (d) Friction coefficient at texture angle of 0° (e) Average friction coefficient at different texture depth.

Figure 16 shows the storage of rubber debris in the micro-grooves at different texture depths without considering the oil delivery capacity of the texture. The reason why the No. 90-5 specimens can obtain the maximum average friction coefficient when the texture angle is 90°, while 0-5, 30-5, and 60-5 were the smallest group of specimens in each experimental group with the same texture angle is because the No.90-5 specimens are worse than the above groups of specimens in terms of oil delivery, and the lubricating medium in the micro-groove is negligible. The deeper the texture depth is, the more is rubber embedded inside the micro-groove, and the more rubber debris is generated by scraping. When the texture depth is too deep, it is difficult to discharge the rubber residues from the contact area, and when the texture depth is too shallow, it cannot completely store the scraping and cutting falling rubber residues. The above factors have a synergistic effect, resulting in the deterioration of the surface contact condition of the friction pair, which in turn makes the friction coefficient increase significantly.

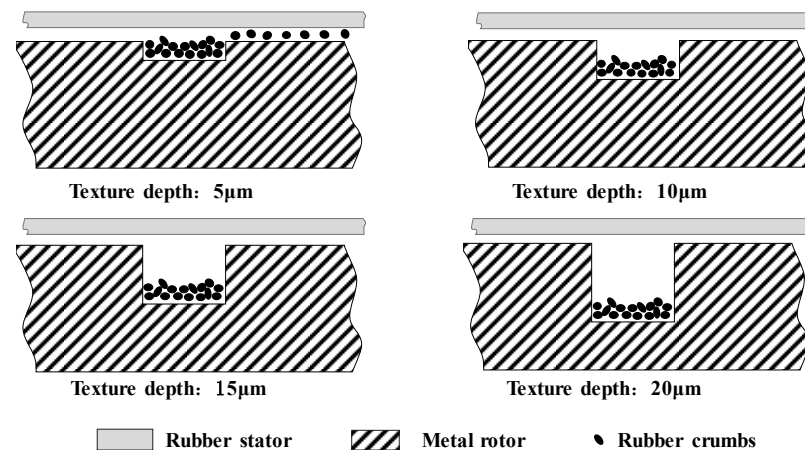


Figure 16. Storage of rubber debris in the texture at different texture depths.

In summary, the effect law of different texture parameters on the friction coefficient in the experiment is basically consistent with the effect law of texture parameters on the lubricating medium delivery capacity and scraping force in the model simulation results, which verifies the accuracy of the simulation results, lays the simulation foundation for subsequent research, and reduces the investment of experimental costs.

3.3. Wear Reduction Mechanism of Texturing in Metal-Rubber Pair of Screw Motors

Table 5 shows the orthogonal test results of the friction coefficients, where K_i represents the sum of the friction coefficients with the level number i in each column, t_i represents the arithmetic mean of the friction coefficients obtained at each level i , and R represents the extreme difference, $R = t_{i(\max)} - t_{i(\min)}$. The larger the value of R , the greater the influence of the factor on the test results. From the extreme difference analysis results, $R_{\text{texture angle}} > R_{\text{texture depth}}$ can be seen, which indicates that in the metal-rubber contact pair, the effect of texture angle on the friction coefficient is greater than that of texture depth. At this time, the test group No. 0-5 obtained the minimum friction coefficient of 0.122.

From the available research results, in the metal matching pair, the wear reduction mechanism of the texture is as follows: (1) Under dry friction conditions, the abrasive particles and debris are stored to improve the contact conditions; (2) Storing lubricant and improving lubrication conditions provides lubricant to the contact surfaces when the lubrication conditions are poor; (3) Under the condition of full oil lubrication, the elastic hydrodynamic lubrication effect can add lift to the oil film and improve the bearing capacity of the oil film.

From Figure 12e, it can be found that in the metal-rubber mating pair studied, the 0° specimen that cannot provide a convergence gap has a smaller friction coefficient than the 90° specimen that can provide a convergence gap. One of the necessary conditions for producing an elastic hydrodynamic lubrication effect is the wedge space that needs convergence. Therefore, it can be determined that the main wear reduction mechanism of the texture is different in the metal-rubber pair and the metal pair. Combined with the effect of texture angle on the lubricating medium passing area in Figure 9 and the extreme difference analysis in Table 5, it can be seen that the oil delivery capacity affected by the texture angle is the main factor in which texture plays a role in reducing wear and resistance in metal-rubber pairings. In addition, as in Figure 6a, a local contact zone exists at its boundary during the period of the beginning of the samples' operation (running-in), which is confirmed by the data from Figure 11 (red zones on the border of the formed grooves). This, in turn, became the reason for the peak increase coefficient of friction at the beginning of the operation of the samples (Figures 12 and 15a–d).

Table 5. Friction coefficient orthogonal test results.

Mark	Factors		Friction Coefficient
	Angle/(°)	Depth/ μm	
Untextured	0	0	0.153
0–5	0(1)	5(1)	0.122
0–10	0(1)	10(2)	0.143
0–15	0(1)	15(3)	0.144
0–20	0(1)	20(4)	0.168
30–5	30(2)	5(1)	0.125
30–10	30(2)	10(2)	0.208
30–15	30(2)	15(3)	0.241
30–20	30(2)	20(4)	0.255
60–5	60(3)	5(1)	0.149
60–10	60(3)	10(2)	0.209
60–15	60(3)	15(3)	0.275
60–20	60(3)	20(4)	0.275
90–5	90(4)	5(1)	0.27
90–10	90(4)	10(2)	0.208
90–15	90(4)	15(3)	0.223
90–20	90(4)	20(4)	0.253
K ₁	0.577	0.666	
K ₂	0.829	0.768	
K ₃	0.908	0.883	
K ₄	0.954	0.951	
t ₁	0.14425	0.1665	
t ₂	0.20725	0.192	
t ₃	0.227	0.22075	
t ₄	0.2385	0.23775	
R	0.09425	0.07125	

4. Conclusions

In this paper, we have established the texture metal-rubber mating plate reciprocating test model based on the spiral matching of hydraulic motor, and carried out the tribological test research for the design of textured depths and textured angles, as well as the simulation research of lubricating medium delivery capacity, and the simulation research of scraping rubber capacity. Using the friction coefficient, lubricating medium flow rate, and rubber surface stress as evaluation indexes, we analyzed the influence law of different texture angles and texture depths on the tribological properties of screw motor friction pairs and obtained the following main conclusions.

(1) The texture angle mainly affects the oil delivery capacity of the micro-grooves in the metal-rubber pair. When the texture direction is consistent with the movement direction, the oil feeding capacity is the strongest, and the texture depth mainly affects the scraping effect of the micro-grooves on rubber, and the deeper the texture, the stronger the scraping effect on rubber.

(2) In the metal-rubber friction pair, the texture angle is the main influencing factor of the friction coefficient. The minimum friction coefficient was 0.122 for a set of specimens with a texture angle of 0° and a texture depth of $5\mu\text{m}$, which was 20.2% lower than that of the untextured treated specimens.

(3) When the design of texture parameters is reasonable, the existence of micro-grooves can effectively improve the tribological properties of the specimen, which is conducive to the smooth start-up of hydraulic motors.

Author Contributions: Conceptualization, S.P. and Z.H.; methodology, S.P. and C.X.; software, S.P. and C.X.; validation, M.W., C.X. and Z.H.; formal analysis, S.P. and C.X.; investigation, S.P. and M.W.; resources, Z.H. and K.C.; data curation, C.X. and K.C.; writing—original draft preparation, S.P. and M.W.; writing—review and editing, Z.H.; visualization, S.P.; supervision, Z.H.; project administration, K.C.; funding acquisition, S.P. and Z.H. All authors have read and agreed to the published version of the manuscript.

Funding: This work is supported by the Nanchong City and Southwest Petroleum University Science and Technology Strategic Cooperation Special Fund (Grant No. SXHZ048), and the Sichuan Province Science and Technology Innovation Miaozi project (Nos. 2022035).

Data Availability Statement: Not applicable.

Acknowledgments: The authors would like to thank the anonymous reviewers for their valuable opinions to improve the manuscript.

Conflicts of Interest: The authors declare no conflict of interest.

References

- Ming, X. Present situation and prospect of oil recovery technology in petroleum engineering. *J. Chifeng Univ. (Nat. Sci. Ed.)* **2018**, *34*, 75–76.
- Jin, X. Present situation and future prospect of petroleum and chemical production technology. *Petrochem. Ind. Technol.* **2019**, *26*, 44–49.
- Yu, C. The current situation of petroleum engineering oil recovery technology and prospect discussion. *Petrochem. Ind. Technol.* **2018**, *25*, 283.
- Gusmanova, A.; Bekbayeva, R.; Koysheva, A.; Koyshev, A. Oil withdrawal technological advancement for multilayer field. *Int. J. Oil Gas Coal Technol.* **2022**, *30*, 265–282. [[CrossRef](#)]
- He, L.I.; Zhongxian, H.A.; Liangang, W.A.; Gang, C. Current technical status and development trend of artificial lift. *Acta Pet. Sin.* **2015**, *36*, 1441–1448.
- Liu, H.; Liu, W.; Lu, Q.; Wang, S. Research status and development trend of deep well production technology. *J. Northeast Pet. Univ.* **2020**, *44*, 1–6, 29, 149.
- Fakher, S.; Khlaifat, A.; Hossain, M.E.; Nameer, H. A comprehensive review of sucker rod pumps' components, diagnostics, mathematical models, and common failures and mitigations. *J. Pet. Explor. Prod. Technol.* **2021**, *11*, 3815–3839.
- Shi, Y.; Wang, M. Characteristics of the formation of bitumen-gum-paraffin deposits on different process equipment in oil recovery systems. *Foreign Oilfield Eng.* **2009**, *25*, 23–46.
- Ilyushin, Y.V.; Fetisov, V. Experience of virtual commissioning of a process control system for the production of high-paraffin oil. *Sci. Rep.* **2022**, *12*, 18415.
- Han, C.J.; Ren, X.Y.; Zheng, J.P. Study on Wear of Stator Bushing of Conventional Progressive Cavity Pump in Heavy Oil Extraction. *Lubr. Eng.* **2018**, *43*, 25–29.
- Liang, Z.Y.; Wang, L.L.; Tang, Z.X. Technology of heavy oil recovered by screw pump combined with water-soluble viscosity in Tahe Oilfield. *Reserv. Eval. Dev.* **2020**, *10*, 111–115.
- Xi, J.C.; An, G.C.; Wang, M.Z. Study on Starting Performance for High-Torque Low-Speed Hydraulic Motors. *China Mech. Eng.* **2008**, *19*, 2929–2933.
- Wang, J.; Wei, S.; Sha, R.; Liu, H.; Wang, Z. Design methodology of a new smooth rotor profile of the screw vacuum pump. *Vacuum* **2019**, *159*, 456–463. [[CrossRef](#)]
- Zhang, X.; Yang, J.; Bei, W.; Han, W.; Chen, C.; Yang, L. Optimal Structure Design and Performance Analysis of Multiphase Twin-screw Pump for Wet Gas Compression: Original papers. *Int. J. Fluid Mach. Syst.* **2021**, *14*, 208–219. [[CrossRef](#)]
- Ye, Z.; Luo, L.; Feng, K.; Yi, Q.; Tan, L. Design and contact characteristics analysis of a new internal twin-screw pump. *Proc. Inst. Mech. Eng. Part C: J. Mech. Eng. Sci.* **2022**, *236*, 7259–7269.
- Wang, R.; Wang, K.H. Microstructure of Plasma Spraying Ceramics Coating Doping Nanometer on Screw-Pump. *J. Southwest Pet. Univ. (Sci. Technol. Ed.)* **2008**, *30*, 143–145.
- Xiao, J.J.; Deng, B.H.; Li, Z.X. Performance Comparison and Application Research of Two Supersonic Flame Spraying Coatings Used for the Positive Displacement Motor. *Mater. Prot.* **2019**, *52*, 174–178.
- Guo, H.; Zhu, C.; Zhao, E.; Yu, P.; Liu, L.; Li, L.; Yang, H. Tribology and corrosion properties of HVOF-sprayed WC coatings on surface of screw pump rotor. *J. Jiangsu Univ. Nat. Sci. Ed.* **2022**, *43*, 332–340.
- Tang, L.M.; Wang, S.J.; Lv, X.R.; Yao, H. Effect of Zinc Oxide on Friction and Wear Behavior of NBR under Dry Sliding. *Polym. Mater. Sci. Eng.* **2016**, *32*, 98–101.
- Han, H.; Wang, S.J.; Lv, X.R. Effect of Surface Modification on Oil Resistance and Wear Resistance of NBR. *China Rubber Ind.* **2015**, *62*, 587–591.
- Zeng, D.; Xu, X.; Wu, J.; Xu, J.; Xue, Y.; Liu, J.; Zhang, M.; Chen, C.; Tian, Y.; Chen, X. Properties of Modified Rubber Powder by Twin-screw Extrusion/NR Blends. *China Rubber Ind.* **2020**, *67*, 839–842.

22. Dang, L.; Wu, W.; Ren, W. The effect of PVC modification on the mechanical properties and media resistance of the stator buna rubber of screw pumps. *Shandong Chem. Ind.* **2016**, *45*, 19–21.
23. Liu, X.J.; Jing, K.N.; Shan, B.; Chen, P. Numerical Simulation Analysis of Stress in Textured Stamping Die. *Surf. Technol.* **2019**, *48*, 9–15.
24. Liu, S.; Sai, Q.; Wang, S.; Williams, J. Effects of Laser Surface Texturing and Lubrication on the Vibrational and Tribological Performance of Sliding Contact. *Lubricants* **2022**, *10*, 10. [[CrossRef](#)]
25. Rosenkranz, A.; Costa, H.L.; Baykara, M.Z.; Martini, A. Synergetic effects of surface texturing and solid lubricants to tailor friction and wear—A review. *Tribol. Int.* **2021**, *155*, 106792.
26. Wang, M.L.; Li, Q.; Huang, Z.Q.; Qian, W.J.; Chen, X.; Li, Q.; Lai, T.H. Influence of surface texture parameters of screw pump rotor on tribological properties of its friction pairs. *Ind. Lubr. Tribol.* **2022**, *74*, 964–974. [[CrossRef](#)]
27. Guo, Y.; Quan, S.; Gong, J.; Liu, D.; Jin, Y.; Yang, S.; Zhang, L. Construction and Numerical Simulation of Energy Consumption Model of High-Frequency Hydraulic Impact Piston with Cylindrical Texture. *Lubr. Eng.* **2020**, *45*, 76–82.
28. Grabon, W.; Koszela, W.; Pawlus, P.; Ochwat, S. Improving Tribological Behaviour of Piston Ring-Cylinder Liner Frictional Pair by Liner Surface Texturing. *Tribol. Int.* **2013**, *61*, 102–108. [[CrossRef](#)]
29. Xu, M.G.; Song, E.Y.; Zhang, H.X.; Cheng, X.; Wu, Z.W. Research on the Cutting Simulation and Experiment of Super-Hard Material Tool with Grooved Micro Texture. *Surf. Technol.* **2021**, *50*, 363–370.
30. Xiao, J.; Zhang, D.S.; Jing, Y.; Gong, J.Y. Lubrication Characteristics of Water Lubricated Stern Tube Bearing with Surface Textured Microgrooves. *Lubr. Eng.* **2020**, *45*, 125–129.
31. Suh, A.Y.; Lee, S.C.; Polycarpou, A.A. Adhesion and Friction Evaluation of Textured Slider Surfaces in Ultra-Low Flying Head-Disk Interfaces. *Tribol. Lett.* **2004**, *17*, 739–749. [[CrossRef](#)]
32. Pettersson, U.; Jacobson, S. Textured Surfaces for Improved Lubrication at High Pressure and Low Sliding Speed of Roller/Piston in Hydraulic Motors. *Tribol. Int.* **2007**, *40*, 355–359. [[CrossRef](#)]
33. Edachery, V.; Shashank, R.; Kailas, S.V. Influence of surface texture directionality and roughness on wettability, sliding angle, contact angle hysteresis, and lubricant entrapment capability. *Tribol. Int.* **2021**, *158*, 106932.
34. Zhang, D.; Sun, X.; Gao, F.; Zhong, S.; Duan, J. Effect of Texture Parameters on Tribological Performance of Slipper Surface in Hydraulic Motor. *Surf. Technol.* **2019**, *48*, 230–236.
35. Li, C.; Yang, X.; Wang, S.; Wang, Y.; Lu, C.; Cao, J. Study on Friction and Lubrication Characteristics of Surface with Unidirectional Convergence Texture. *Coatings* **2019**, *9*, 780. [[CrossRef](#)]
36. Su, F.H.; Mao, C.; Li, Z.J. Experiment and Simulation Study on the Effect of Texture Depth on Tribological Properties of Stainless Steel Surface under Oil Lubricating Condition. *Tribology* **2019**, *39*, 181–187.
37. Liu, S.S.; Liu, Q.; Liu, J.G.; Jiang, S.Q.; Liao, J.H.; Yu, J.; He, J.G. Synergistic Antifriction Mechanism of Surface Micro-Textured Graphite Coating on Aluminum Alloy Surface. *Surf. Technol.* **2019**, *48*, 29–38.
38. He, X.; Liao, W.L.; Wang, G.R.; Zhong, L.; Jiang, L. Influence of Edges Bulge of Texture on Tribological Performances of Plunger-Seal Pair in Fracturing Pump. *Lubr. Eng.* **2016**, *41*, 96–101.
39. Xu, Z.; Xue, S.; Wang, C.; Wang, X.; Xu, J.; Shan, D.; Guo, B. Electrically assisted micro-rolling process of surface texture on T2 copper sheets. *Int. J. Adv. Manuf. Technol.* **2021**, *118*, 2453–2466.
40. Wu, Z.; Bao, H.; Xing, Y.; Liu, L. Tribological characteristics and advanced processing methods of textured surfaces: A review. *Int. J. Adv. Manuf. Technol.* **2021**, *114*, 1241–1277.
41. Dzyura, V.; Maruschak, P. Optimizing the Formation of Hydraulic Cylinder Surfaces, Taking into Account Their Microrelief Topography Analyzed during Different Operations. *Machines* **2021**, *9*, 116. [[CrossRef](#)]
42. Dzyura, V.; Maruschak, P.; Slavov, S.; Gurey, V.; Prentkovskis, O. Evaluating Service Characteristics of Working Surfaces of Car Parts by Microgeometric Quality Parameters. *Machines* **2021**, *9*, 366. [[CrossRef](#)]
43. Zhang, H.; Hua, M.; Dong, G.N.; Zhang, D.Y.; Chin, K.S. A Mixed Lubrication Model for Studying Tribological Behaviors of Surface Texturing. *Tribol. Int.* **2016**, *93*, 583–592. [[CrossRef](#)]
44. Yan, Z.; Sun, J.Y.; Jiang, D.; Wang, D.; Quan, X.; Weng, L. Tribological Behavior of Laser Textured TiN Films under Dry Friction Condition. *Tribology* **2017**, *37*, 518–526.
45. Sedlaček, M.; Podgornik, B.; Ramalho, A.; Česnik, D. Influence of Geometry and the Sequence of Surface Texturing Process on Tribological Properties. *Tribol. Int.* **2017**, *115*, 268–273. [[CrossRef](#)]
46. Wang, J.Q.; Wang, X.L. State of the Art in Innovative Design of Surface Texture. *J. Mech. Eng.* **2015**, *51*, 84–95. [[CrossRef](#)]

Disclaimer/Publisher's Note: The statements, opinions and data contained in all publications are solely those of the individual author(s) and contributor(s) and not of MDPI and/or the editor(s). MDPI and/or the editor(s) disclaim responsibility for any injury to people or property resulting from any ideas, methods, instructions or products referred to in the content.